

**LLNL DETECTION PROGRAM: BROAD AREA CHARACTERIZATION OF PHASE
DETECTABILITY AND EMPIRICAL DETECTORS FOR SPECIFIC SOURCES**

David B. Harris, William R. Walter, Arthur J. Rodgers, Alan Sicherman, Stephen Myers and Craig Schultz

Lawrence Livermore National Laboratory

Sponsored by National Nuclear Security Administration
Office of Nonproliferation Research and Engineering
Office of Defense Nuclear Nonproliferation

Contract No. W-7405-ENG-48

ABSTRACT

LLNL detection research addresses two technical issues: detectability of seismic phases over broad regions and specialized algorithms for detecting events originating at specific sources. The detectability of seismic phases underpins the applicability and performance of discrimination and location algorithms by determining which phase observations are likely to contribute to discriminant and event location calculations. Seismic phase detectability is a function of expected phase signal-to-noise ratio (SNR), which, for a particular station, is a function of the phase amplitude spectrum and the noise spectrum at the station. We represent (map) phase amplitudes over broad regions for any given station with empirical (kriged) corrections superimposed on base values determined from an MDAC model. MDAC, which stands for Magnitude Distance Amplitude Correction, is a phase amplitude model that combines a source spectrum model, geometric spreading and attenuation. Ultimately, phase amplitude maps and station noise spectra will determine the geographic distribution of phase observation probabilities. These probabilities, in turn, determine the likelihood that data for particular discriminants will be available and should allow the construction of maps delimiting the geographic range of applicability of those discriminants.

The second technical issue concerns the detection of events occurring at discrete sources, such as mines. This issue is of monitoring interest because mining explosions must be discriminated from earthquakes and nuclear explosions. The need for an efficient screen is particularly acute in mining districts, where explosions dominate event detections at observing stations. The same screening technique can be used to build reference populations of explosions for designing and testing other discriminant algorithms. Frequently, mining sources produce repetitive signals, a signal structure that can be exploited to increase dramatically the probability of detection at a given false alarm rate. The classical solution to problems of detecting known signals is the matched filter, which correlates a template waveform against a continuous data stream to detect occurrences of that waveform. However, signals from repetitive seismic sources often exhibit significant variation that degrades matched filter performance. Our solution to this problem is to use subspace detectors, which replace the matching template with a suite (subspace) of templates that are combined linearly to match occurrences of variable signals from a particular source. We outline template subspace design procedures that maximize the probability of detection for a fixed false alarm rate by varying the dimension of the subspace.

KEY WORDS: seismic detection, phase detectability, signal-to-noise ratio, subspace detectors

OBJECTIVE

Phase Detection and Measurement over Broad Regions

Location and identification of seismic events rely on the ability to detect seismic phases with sufficient signal-to-noise to allow measurements of phase arrival times and amplitudes. However, geometric spreading, heterogeneous attenuation, other variable propagation characteristics of the earth and variations in noise properties cause signal detection characteristics to vary greatly geographically and with frequency.

Seismic identification relies on observations of high-frequency seismic phases to form amplitude, spectral- and cross-spectral ratios for comparison with measurements from events of known source type. Thus, phases must be observed with sufficient signal-to-noise to form meaningful discriminant measurements.

In order to quantify the probability of observing regional phases, we are developing a strategy for characterizing station-specific signal detection as a function of event size, distance, frequency and path. Our characterization depends on the magnitude distance amplitude correction (MDAC) that provides a theoretical model for regional phase amplitudes as a function of frequency, event size (moment magnitude) and distance. Empirical corrections for path effects are estimated by kriging MDAC residuals. The MDAC model parameters, amplitude residual correction surfaces and noise properties at a specific station provide the data from which detection characteristics can be derived.

Subspace Detectors

The objective of subspace detector design is to maximize the probability of detecting variable signals from a particular source for a fixed false alarm rate. Subspace detectors provide a mechanism for detecting signals exhibiting a degree of variation by assuming that the signals to be detected can be represented as a linear combination of basis waveforms. The basis is derived from collections of master event waveforms recorded for events generated by the source of interest and is conveniently represented by a projection operator. The probabilities of detection and false alarm can be traded off by varying the threshold of the detector and the design of the projection operator. Our FY01 research has focussed on determining the statistics of the detector and the dependence of the statistics on the projection operator. This knowledge leads to a projection operator design strategy for maximizing the performance (probability of detection) of a subspace detector.

RESEARCH ACCOMPLISHED

Our seismic detection research is directed in two major areas: regional phase signal-to-noise modeling and source-specific empirical detection. Research accomplished in these areas is described below.

Regional Phase Signal-to-Noise and Detection

Recent advancements in modeling high-frequency (0.5-10 Hz) regional phase amplitudes allows for a predictive model of Pn, Pg, Sn and Lg amplitude spectra for events of a given size and distance (Taylor and Hartse, 1998; Taylor et al., 2002, Walter et al. this Proceedings). This MDAC2 model represents the spectrum of each phase as a convolution of a source spectrum, geometric spreading, attenuation, and site terms. The source model is a generalized Brune (1970) model that accounts for corner frequency -moment scaling. An apparent attenuation law, $Q(f) = Q_0 f^{-\gamma}$ and a geometric spreading exponent, are used for each phase. The theoretical approach has been recently enhanced to allow for non-constant apparent stress and differing P- and S-wave source corner frequencies (Walter and Taylor, 2001). Examples of MDAC2 spectral fits to Nevada Test Site (NTS) earthquake data are shown in Walter et al (this Proceedings).

Using the attenuation parameters discussed in Walter et al (this Proceedings) we can calculate synthetic MDAC2 predicted spectra for a hypothetical earthquake of $M_w=3.0$ at NTS and ask about its detectability at primary IMS station MNV (~200 km) and auxiliary station ELK (~400km). Taking a ratio of the synthetic MDAC spectra to a noise spectrum at each station we can make predicted signal-to-noise spectra for each phase as shown in Figure 1 below.

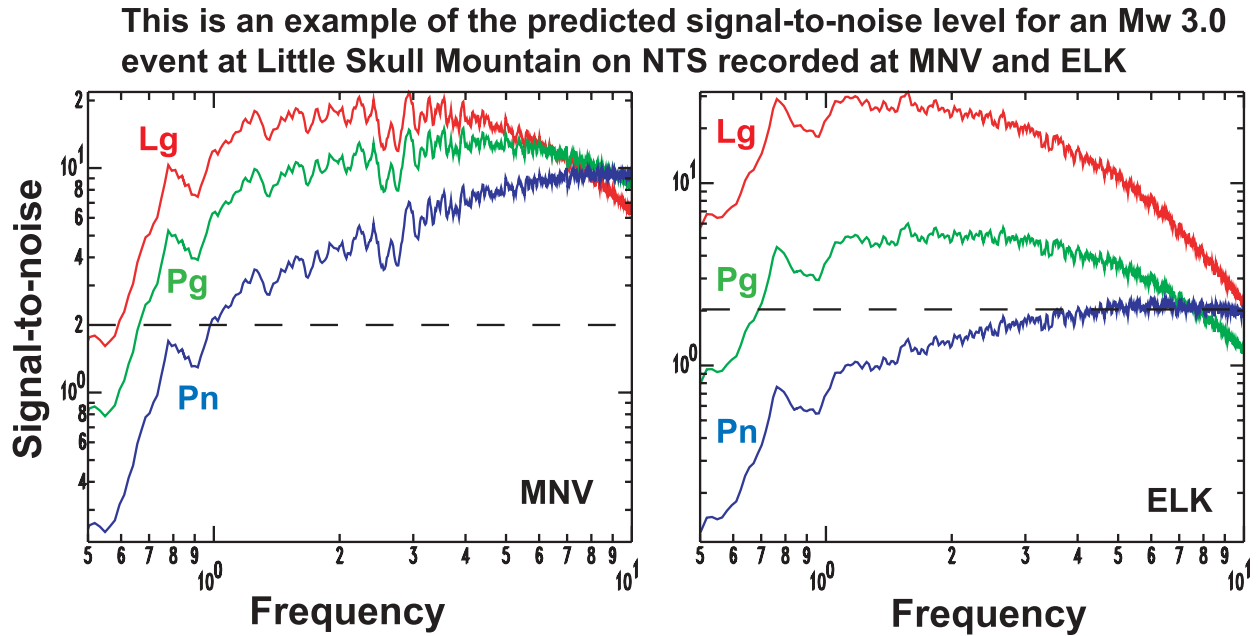


Figure 1. Predicted signal-to-noise spectrum for an Mw=3.0 earthquake near Little Skull Mountain on NTS at station MNV and ELK. The dashed line shows a SNR value of two. Note that at MNV all 3 phases look detectable above about 1 Hz while at the more distant station ELK Pn is probably only detectable above 4 Hz and Pg and Lg may not be detectable above 7 Hz and 10 Hz respectively.

One important caveat to these predictions of signal to noise is that since it was derived from an earthquake source model, it will have to be modified before being applied to explosions. For example, an explosion may generate larger P-waves (Pn,Pg) and smaller S-waves (Sn, Lg) than an earthquake of the same magnitude; if so, this will affect detectability. We are planning to incorporate an explosion source model as an option in future updates of MDAC.

We have applied these techniques to other regions, for example a regional dataset of mb \leq 3.5 events recorded at station NIL in Pakistan. A subset of high SNR data was fit using MDAC in a grid search routine. After MDAC parameters for all four phases at a station are found, the predicted amplitude in specific frequency bands (e.g. 1-2, 2-4, 4-6 Hz) is subtracted from the observed amplitude to form amplitude residuals. These residuals are projected to the event location and are used to create empirical amplitude correction surfaces with the Bayesian kriging algorithm (Schultz et al., 1998; Rodgers et al., 1999; Phillips, 1999). Figure 2 shows the kriged MDAC residual amplitudes. This figure shows that Lg propagates more efficiently from southern and southeastern azimuths and less efficiently from western and eastern azimuths. Path specific amplitude effects will clearly have a direct impact on phase detection.

We can also estimate the average noise spectrum from this same dataset. The average noise spectra are computed by stacking 565 pre-Pn noise samples, each 35 second long and ending 5 seconds before the analyst picked P-wave arrival. Noise uncertainties are taken as two standard deviations from the mean. Detection of the phase may be possible when the predicted amplitude at a specified frequency falls above the noise model. We combined the MDAC and kriging corrections with the noise model to create laterally varying signal-to-noise surfaces that can then be used as input for probabilistic calculations of signal detection. Figure 3 shows the estimated signal-to-noise for Lg 1 to 2Hz at station NIL for both the laterally homogeneous MDAC correction and the laterally heterogeneous MDAC + kriging path correction. We computed Lg 1- to 2-Hz signal-to-noise as the log base-10 MDAC-predicted amplitude minus the noise. For the noise model we took a conservative approach and used twice the standard deviation above the mean model. For the laterally heterogeneous case, this figure shows that the estimated signal to noise for Lg 1 to 2 Hz is above 2:1 (0.3 log base-10) for distances of nearly 1500 km to the southeast. But for distances greater than 1000 km to the east and west, the estimated signal to noise for Lg 1 to 2

Hz is below 2:1; thus, accounting for the lateral variations is important for more accurate spatial estimates of detectability.

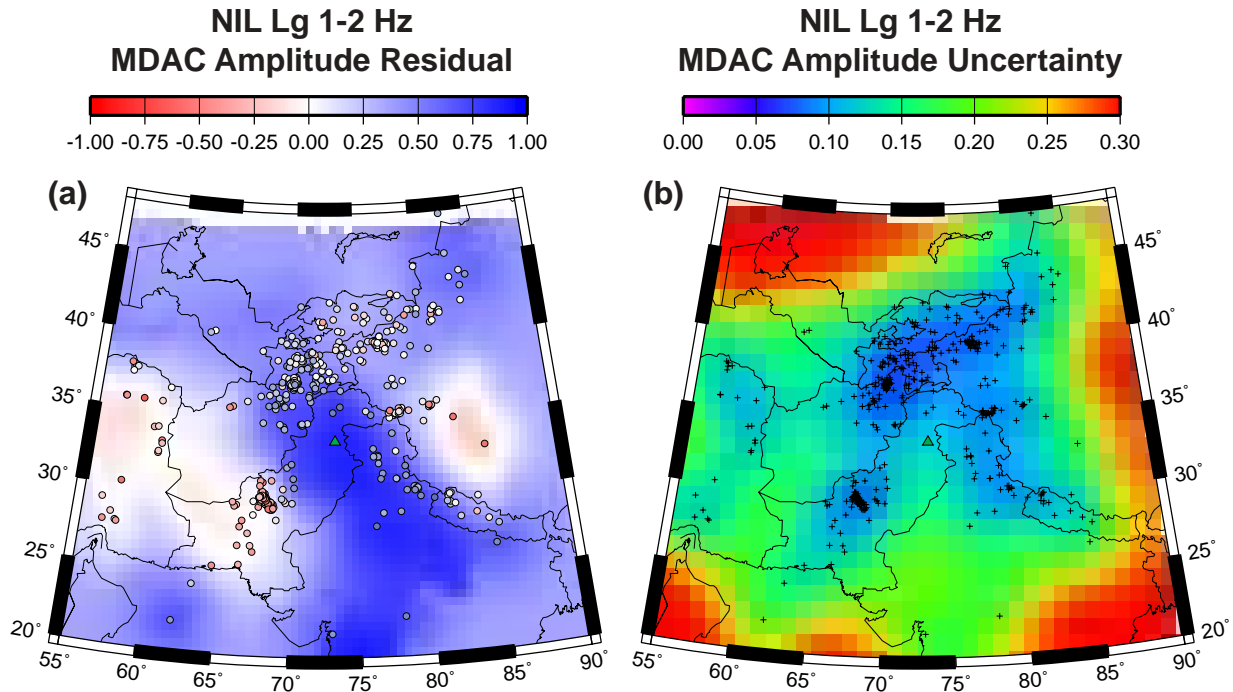


Figure 2 (a) MDAC residuals (circles for Lg 12 Hz at station NIL (Nilore, Pakistan) plotted on top of the amplitude correction surface estimated from Bayesian kriging (Schultz et al., 1998). (b) Uncertainty from kriging algorithm.

A more detailed and comprehensive picture of signal detection comes from doing probabilistic calculations in addition to using estimated values. The probabilistic calculations address the uncertainties in signal to noise for an event of a given magnitude and location with respect to a monitoring station. An approach we have employed to address these uncertainties is to take an earthquake data set and use a linear regression model of the following form for any particular phase:

$$\log_{10}(\text{signal to noise}) = A_1 + B_1 M_w + C_2 r + C_3 \log_{10}(r) + \epsilon$$

where r is the distance to the station, M_w is moment magnitude, and ϵ is assumed to be normally distributed with mean 0 and variance σ_1 . The parameters C_2 and C_3 come from the MDAC amplitude model and are treated as known, while the other parameters come from the linear regression fit. This kind of model is similar in spirit to that found in Taylor and Hartse, 1996, and Sereno and Bratt, 1989. The above model is laterally homogeneous (or 1-D) as denoted by the numerical subscript of 1 on the parameters from the regression fit.

We have extended this model concept to address the laterally heterogeneous case as follows:

$$\log_{10}(\text{signal to noise}) = A_2 + B_2 M_w + C_2 r + C_3 \log_{10}(r) + D_2 \text{kriging correction} + \epsilon$$

where kriging correction is the kriging correction from the MDAC model as illustrated previously in Figure 2, and ϵ is assumed to be normally distributed with mean 0 and variance σ_2 . The subscript 2 on the parameters from the regression fit indicate that this is a 2-D model. Since lateral variability is reflected by the kriging correction term, σ_2 is less than σ_1 . As discussed below, this can result in improved confidence in detection.

NIL Lg 1-2 Hz Predicted Signal-to-Noise for a Mw=4.0 Earthquake

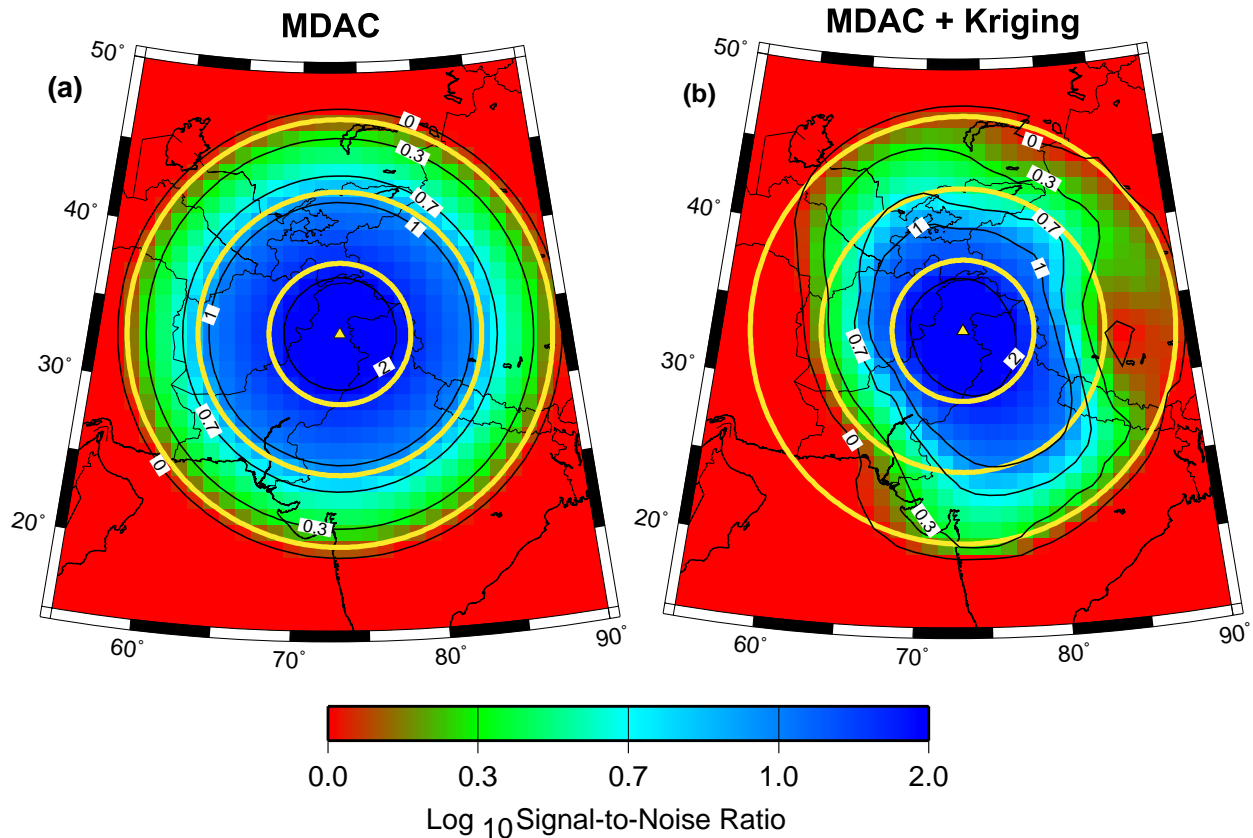


Figure 3. (a) Lg 1-2 signal-to-noise predicted from the MDAC model and the average noise at station NIL. (b) Lg 1-2 signal-to-noise predicted from the MDAC + kriging amplitude path correction. Signal-to-noise ratios less than 1.0 (log_{10} 0.0) are plotted in red. Yellow circles are plotted at 500, 1000 and 1500 km from station NIL (yellow triangle).

These regression models allow us to construct new figures similar in spirit to the laterally homogeneous and heterogeneous figures above, but which incorporate effects of uncertainties. For example, the regression models can be used to compute the moment magnitude for which we have 90% confidence of detecting a SNR of at least 2:1 as a function of spatial location. The laterally homogeneous model will show radial symmetry about the station, but requires larger moment magnitudes to satisfy the 90% confidence criterion the larger the σ_1 . The laterally heterogeneous model has a reduced variance due to the kriging correction term. This can lead to significantly smaller moment magnitudes that satisfy the 90% confidence criterion for the same distance from the station. However, for spatial locations where the kriging correction shows poor signal-to-noise propagation, detection performance will be degraded.

Other insights can be gained by holding different variables fixed and plotting a selected variable as a function of spatial location. In the discussion above, the probability of detection was fixed at 90%, the SNR threshold was set at 2:1, and the moment magnitude was plotted as a function of spatial location. We can also fix the moment magnitude at a fixed level (e.g., 4.0, 3.5, etc.) and plot the probability of detection as a function of spatial location for any selected phase. Comparing the laterally homogeneous and heterogeneous cases reveals insights similar to the example above.

We have also extended the probabilistic models for examining a single phase, to examine the simultaneous detectability of multiple phases such as Pg and Lg both having SNRs, above, say, 2:1. Once the models for individual phases were calibrated, we developed a joint detectability model that is multivariate normal with mean

μ and covariance matrix Σ . The vector μ is the vector mean of the \log_{10} (signal to noise) for each phase as a function of distance and moment magnitude obtained from the regression models for individual phases. The matrix Σ is the covariance matrix of the ϵ s from those same models. This multivariate normal distribution was used to compute the probability of detecting multiple phases all above a signal-to-noise ratio threshold for a given magnitude and location from a station. Using this model, a figure showing the spatial dependency of probability of detection for, say, both P_g and L_g as a function of magnitude and location can be constructed as was done for a single phase.

In summary, by incorporating kriging corrections into detectability models, we can characterize our capability in a more spatially accurate manner. This increased accuracy can lead to improved confidence for detecting lower magnitude phases at the same distance from a station than would have been estimated without the kriging corrections. We have also extended the models to estimate the joint detectability of multiple phases.

Subspace Detectors

The subspace detector (Scharf and Friedlander, 1994) provides a flexible, yet sensitive detector for signals that exhibit variation within a linear space of basis waveforms. It replaces the single waveform template of the matched filter, with the more general signal representation as a linear combination of a suite of templates. Like all detectors, the subspace detector implements a binary hypothesis test on a window that slides along a continuous data stream (see Figure 4). In the null hypothesis (H_0), the data in the window, represented by vector \underline{x} , are assumed to consist of noise, assumed to be a white, zero-mean, stationary Gaussian random process with unknown variance (power level) σ^2 . Under the alternative hypothesis (H_1) the data are assumed to consist of signal plus noise. In the subspace detector, the signal is a deterministic mean in the probability model, and is assumed to be the product of a matrix of orthonormal templates (column vectors) \underline{U} and a vector of unknown weights \underline{a} . The principal design issue is to choose the number of columns of \underline{U} (dimension d) and to define the column vectors.

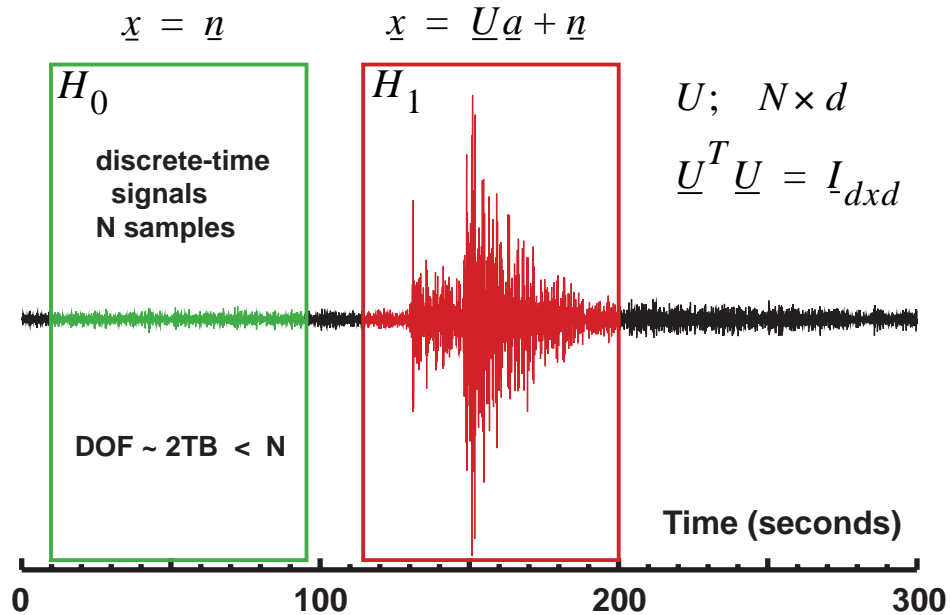


Figure 4 The subspace detector implements a binary hypothesis test on the presence or absence of a signal in background Gaussian noise of unknown variance. The signal is assumed to be a deterministic mean in the probability model and satisfying a parametric model Ua , with unknown parameters a . The unknown signal and noise parameters are estimated from the data to implement the detector as a generalized likelihood ratio test (GLRT).

A likelihood ratio test is implemented to determine which hypothesis (signal / no signal) is correct. The likelihood ratio contains initially unknown parameters (\underline{a}, σ^2), which are estimated from the data. The resulting decision rule is called a generalized likelihood ratio test. The detector implements an intuitive projection operation: the vector of data in the detection window are projected onto the matrix of signal templates. Only when the projection is large is a detection declared. The projection operation is normalized so that the key (sufficient) statistic resembles a correlation coefficient:

$$z = \frac{\underline{x}^T \underline{U} \underline{U}^T \underline{x}}{\underline{x}^T \underline{x}}$$

The operator defining a subspace detector represents a collection of defining waveforms from events at a particular source. Figure 5 displays an example set of 32 aligned signals (vertical channel) observed by Mednet station GFA, and generated by explosions at a phosphate mine near Gafsa, Tunisia. These waveforms were obtained by clustering a larger set of detections with a single link algorithm using a waveform correlation distance measure. The projection operator is a low-dimensional, orthonormal basis for the reference waveforms characterizing the source. To calculate the basis, the reference waveforms are organized as columns of a data matrix \underline{X} , an SVD of the matrix is computed, and the matrix of left singular vectors is partitioned into a d -dimensional representation matrix, \underline{U}_d , corresponding to the largest singular values and an $(N-d)$ -dimensional matrix, \underline{U}_e , spanning residual signals.

The accuracy of the representation provided by the basis waveforms increases with increasing dimension; representation accuracy can be conveniently measured by the fraction (f) of the total signal energy captured by the low-order representation. Figure 6 shows the fractional energy capture for all 32 events in Figure 5 as a function of representation order. Dimension $d=10$ provides approximately 90% energy capture for all events, and is a suitable representation for the signals generated by this particular source.

Probability distributions for the detection statistic z can be used to compute the subspace detector probability of detection for a fixed false alarm rate. These distributions in turn can be used to optimize the detector by maximizing the probability of detection as a function of the dimension d of the subspace representation. This capability leads to an important design strategy. The detection statistic z can be shown to be central beta distributed with $N-d$ and d degrees of freedom under the null hypothesis (H_0 : noise only), i.e. $z \sim \beta(N-d, d)$. N is the number of degrees of freedom in the data (roughly the number of independent data samples). The distribution is doubly non-central beta under the alternative (H_1 : signal + noise) hypothesis when energy capture is less than perfect (i.e. $f < 1$): $z \sim \beta(N-d, d, fE/\sigma^2, (1-f)E/\sigma^2)$.

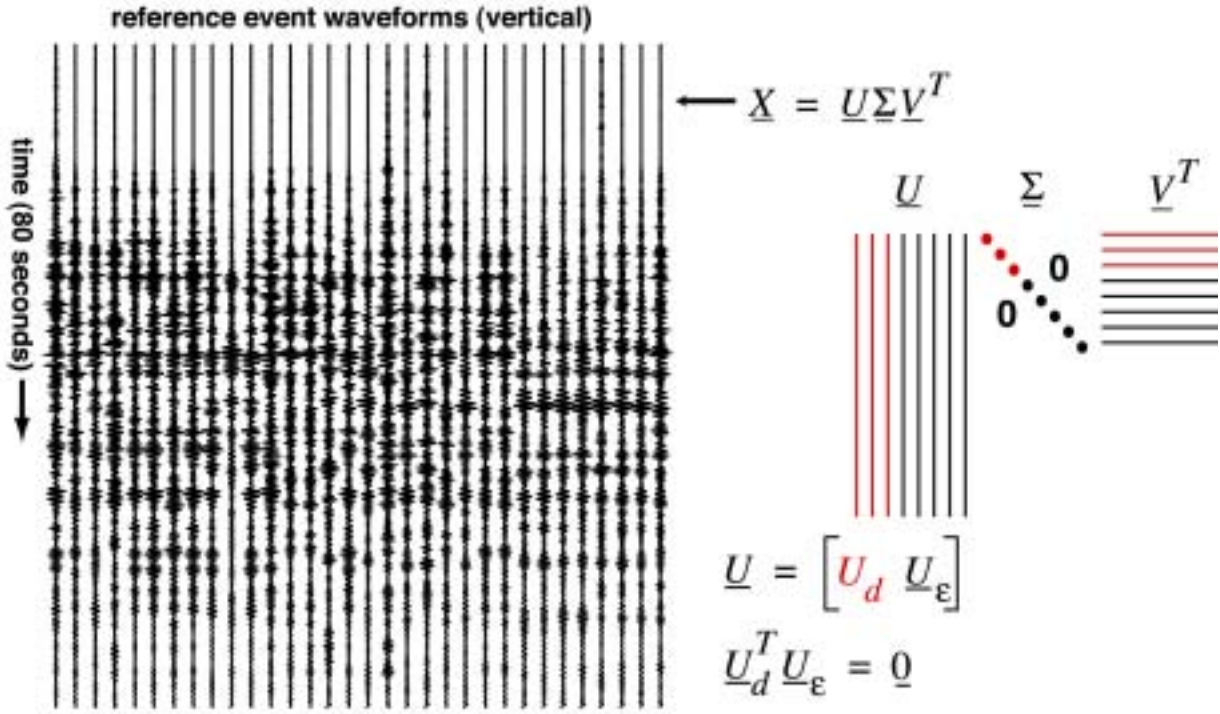


Figure 5 The subspace projection operator U_d is computed from reference waveforms from a particular source. This figure shows 32 waveforms recorded by Mednet station GFA (Tunisia) for explosions at one particular mine in the Gafsa phosphate mining district. The waveforms are aligned and stacked in a data matrix; an SVD is used to extract a lower-dimensional (d) matrix of basis waveforms.

The suite of curves in Figure 7 shows how the detection statistic may be optimized to maximize the probability of detection. The figure shows normalized probabilities of detection as a function of post-integration SNR for subspace detectors with dimensions ranging from 1 to 15. These curves are computed using the energy capture curve shown in red in Figure 6 for one of the 32 reference events. The probability curves have been normalized by the probability of detection for a simple energy (STA/LTA) detector operating on the same detection window with the same false alarm rate. Hence, the curves indicate the relative performance of subspace detectors compared to a simple energy detector. Subspace detectors integrate signal energy over all frequencies coherently, whereas the energy detector, with no knowledge of the signal temporal structure, integrates energy incoherently. Consequently, the curves of Figure 7 demonstrate coherent processing gain.

The best performance is attained for subspace detectors with dimensions of 9 or 10, and in a finite range of post-integration SNR. Performance varies as a function of subspace dimension, because more and more signal energy is processed coherently (captured) as subspace dimensions increases. Beyond dimension 10, the subspace operator captures little additional signal energy, but captures more and more noise energy, causing performance to degrade. Processing gain varies dramatically with SNR and is maximized in the threshold-operating region of STA/LTA detectors for the simple reasons that neither detector performs well at SNRs approaching zero, and both perform very well at high SNRs. Subspace detectors perform very well in the crucial region of threshold detection.

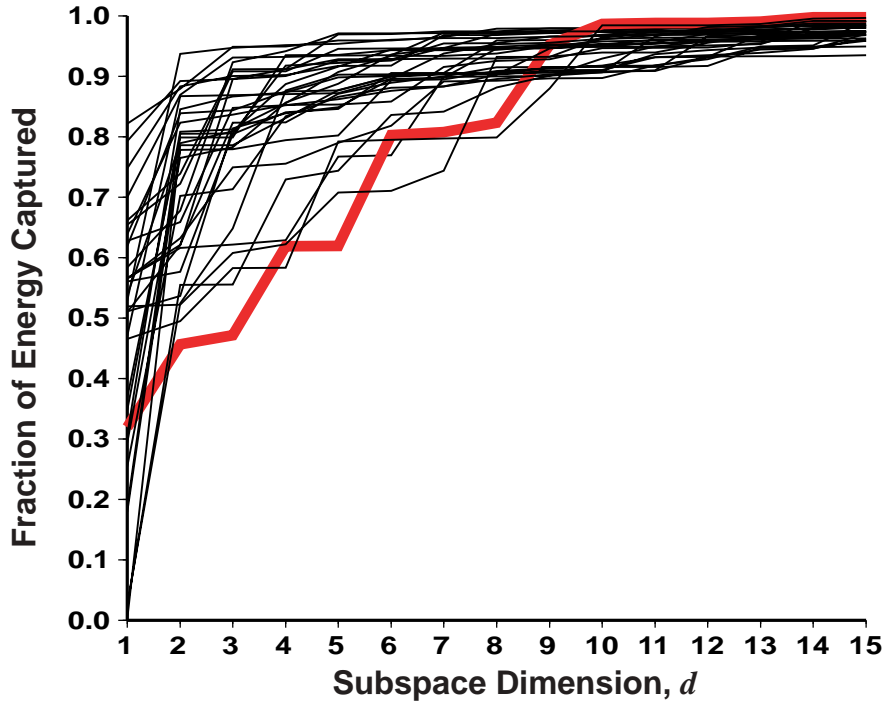


Figure 6 These curves depict the fraction of energy in each of the 32 signals in Figure 5 captured by the low-dimensional subspace representation. The fraction of energy captured by the representation is a function of the dimension d of the subspace.

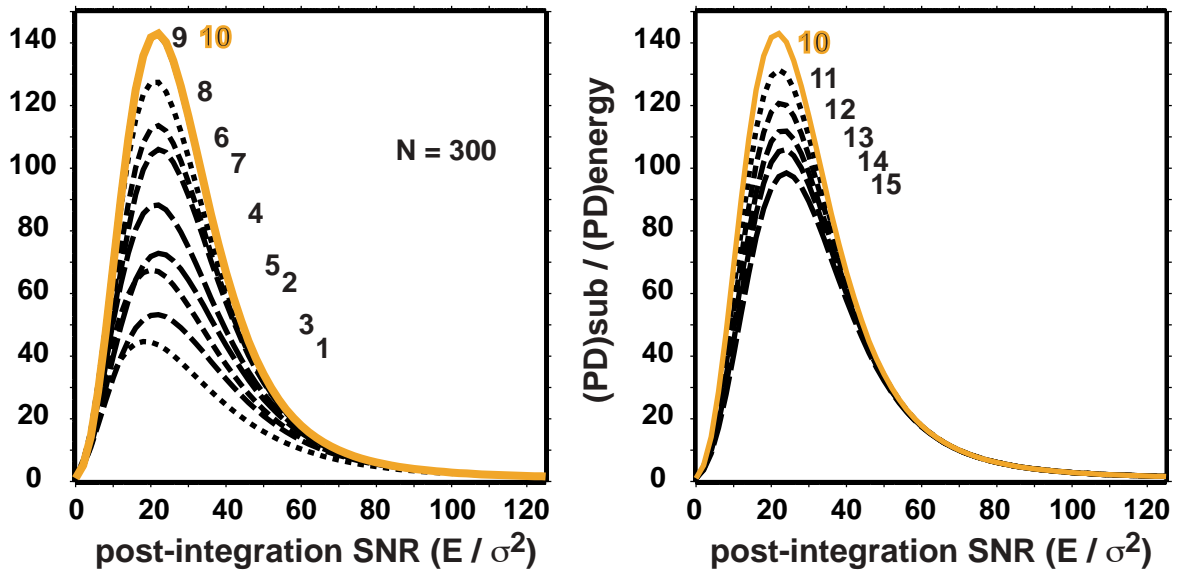


Figure 7 These curves show the normalized probabilities of detection for a range of subspace detectors for a single event waveform (the one indicated in red in Figure 6), at a fixed false alarm probability of 0.0001. The probabilities of detection for the subspace detectors of dimensions $d=1$ through $d=15$ are here divided by the probability of detection for a comparable energy (STA/LTA) detector, and the resulting ratio is plotted as a function of post-integration signal-to-noise ratio. Thus, the curves represent coherent subspace detector processing gain over a simple incoherent detector. The subspace probability of detection is maximum for a dimension of 10, indicating the optimum subspace dimension for this particular event.

CONCLUSIONS AND RECOMMENDATIONS

We have outlined here a methodology to quantify our ability to detect regional seismic phases. The method uses an MDAC spectral model, kriged residuals and a probabilistic model. As MDAC calibration and empirical data collection occurs at each station the detection model will improve. This methodology is important in deciding which phases and frequency bands will be available to locate and discriminate an event at a given station. In turn this procedure guides the choice of particular detection or location algorithms. Finally a quantifiable detection model such as outlined here is crucial for assessing the overall monitoring capability of particular stations.

In addition, we have outlined a method for choosing projection operators in subspace detectors to maximize the probability of detection at a fixed false alarm rate. This procedure provides a rational basis for selecting the order (representation accuracy) of the subspace projection operator. In the future, we plan to deploy this design procedure for the numerous mining sources in northern Fennoscandia and Russia observed by the ARCESS array.

REFERENCES

- Phillips, W. S. (1999). Empirical path correction for regional-phase amplitudes, *Bull. Seismo. Soc. Amer.*, **89**, 384-393.
- Rodgers, A., W. Walter, C. Schultz, S. Myers and T. Lay (1999). A comparison of methodologies for representing path effects on regional P/S discriminants, *Bull. Seismo. Soc. Amer.*, **89**, 394-408.
- Scharf, L. L. and B. Friedlander (1994). Matched subspace detectors. *IEEE Trans. on Signal Processing*, **42(8)**, 2146-2157.
- Schultz, C., S. Myers, J. Hipp and C. Young (1998). Nonstationary Bayesian kriging: application of spatial corrections to improve seismic detection, location and identification, *Bull. Seism. Soc. Am.*, **88**, 1275-1288.
- Sereno, T. and S. Bratt (1989). Seismic detection capability at NORESS and implications for the detection threshold of a hypothetical network in the Soviet Union, *J. Geophys. Res.*, **94**, 10,397-10,414.
- Taylor, S. and H. Hartse (1996). Regional phase detection thresholds at WMQ, Los Alamos National Laboratory, Los Alamos, New Mexico, LAUR-96-395.
- Taylor, S. and H. Hartse (1998). A procedure for estimation of source and propagation corrections for regional seismic discriminants, *J. Geophys. Res.*, **103**, 2781-2789.
- Taylor, S., A. Velasco, H. Hartse, W. S. Phillips, W. Walter and A. Rodgers (2002). Amplitude corrections for regional seismic discriminants, *in press PAGEOPH Special Volume on Seismic Discrimination for CTBT Research*.
- Walter, W. R., and S. R. Taylor, A revised magnitude and distance amplitude correction (MDAC2) procedure for regional seismic discriminants, Lawrence Livermore National Laboratory, UCRL-ID (in prep.), 2001.